ACS APPLIED BIO MATERIALS

www.acsabm.org Article

Light-Induced Caspase-3-Responsive Chimeric Peptide for Effective PDT/Chemo Combination Therapy with Good Compatibility

Yong-Li Mu,[#] Jin Zhang,[#] Meng-Qing Xu, Mohamed F. Foda, Yang Wu, and He-You Han*

Cite This: https://dx.doi.org/10.1021/acsabm.0c00122 Read Online

ACCESS | Metrics & More | Article Recommendations | Supporting Information

ABSTRACT: Activated doxorubicin (DOX) often has severe systemic toxicity and side effects due to its inability to distinguish tumor cells from normal cells, which seriously affects the prognosis of patients. Here, we synthesized an inactivated a DOX prodrug that could be selectively activated by a light-induced caspase-3 enzyme in the tumor site. In the absence of light, this uniformly dispersed nanoparticle avoided the unnecessary toxicity under physiological conditions. Upon the laser irradiating to the tumor area of interest, the nanoparticles can produce a large amount of reactive oxygen species (ROS) to induce cell apoptosis and activate caspase-3 enzyme to release DOX selectively. Meanwhile, the produced ROS can also combine with activated DOX to cause more potent tumor damage. The experiments demonstrated that the light can effectively activate DOX drug through a series of cascade events and the subsequent synergistic therapy both *in vitro* and *in vivo*. This strategy achieved excellent therapeutic outcomes and minimal adverse effects, which should significantly improve the dilemma of traditional chemotherapy.

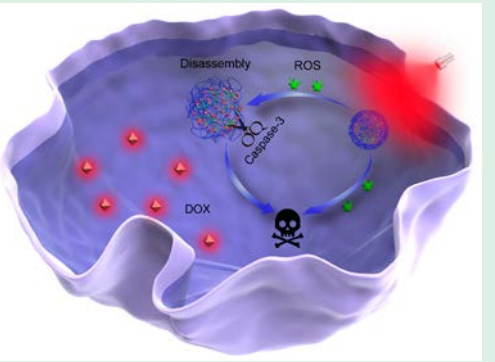

KEYWORDS: *caspase-3-responsive, prodrug activation, tumor target, systemic toxicity, combined therapy*

INTRODUCTION

Small-molecule chemotherapy drugs are still used as a basic clinical treatment.[1,2] However, their indiscriminate toxicity is a double-edged sword with severe side effects. To overcome these issues, some researchers have developed many drug delivery systems (DDSs) to improve tumor targeting and control their releases, such as liposomes,[3] polymers,[4] peptides,[3] and inorganic nanoparticles.[5] Most active drugs were loaded directly by hydrophobic interaction and physical absorption.[6,7] Although they avoided direct contact between the drugs and normal tissues to some extent, there was still leakage of active drugs due to the unstable nanostructure and interaction force, which would cause unnecessary damage at the normal sites. To further compensate for this deficiency, others constructed some small-molecule prodrugs through covalent interaction that could be selectively activated by specific tumor microenvironments, such as an overexpressed enzyme,[8] pH,[9] GSH,[10] and hypoxia.[11] However, specific normal tissues could also express enzymes/receptors at a relatively low level, which would cause the inappropriate prodrug activation and the subsequent systemic toxicity. Compared with the above complex physiological microenvironments, the controllable external stimulus, light, might be an ideal choice as the high spatial and temporal properties.[12,13] It is well-known that the long-wavelength light was more suitable for biological applications than short-wavelength light because of the lower tissue absorption and higher penetration depth.[14] However, another problem with long-wavelength light is that it is challenging to break the high-energy covalent bonds directly. Given this fact, other indirect activation strategies have been developed by coupling a reactive oxygen species (ROS) responsive linker and photosensitizer molecule in the near-infrared (NIR) region.[15,16] This strategy could not only reduce the side effect but also be applied for chemo-PDT combination therapy.[17−19] It is worth noting that the breakage of a ROS responsive linker would also consume a large amount of ROS, which would impair the efficiency of PDT. Therefore, it is necessary to construct a DDS for efficient PDT/chemo combination therapy with minimal side effects and ultrahigh biocompatibility.

Keeping all these issues in mind, here, we synthesized a simple photosensitizer−anticancer drug conjugate (phDD) by using a light-induced caspase-3-responsive peptide sequence as a linker to connect doxorubicin (DOX) and pheophorbide-a (pha) to the two ends of the peptide chain, respectively. What's more, activating this trigger only after PDT can minimize side effects without compromising photodynamic

Received: February 3, 2020
Accepted: March 9, 2020
Published: March 9, 2020

https://dx.doi.org/10.1021/acsabm.0c00122
ACS Appl. Bio Mater. XXXX, XXX, XXX−XXX

Scheme 1. (a) phDD Molecules Self-Assemble into Spherical Nanoparticles under Physiological Conditions and (b) phDD Nanoparticles Produced ROS under the Conditions of Light Irradiation and Activated Caspase-3 Enzyme to Further Release DOX for Combined Therapy in Tumor Cells

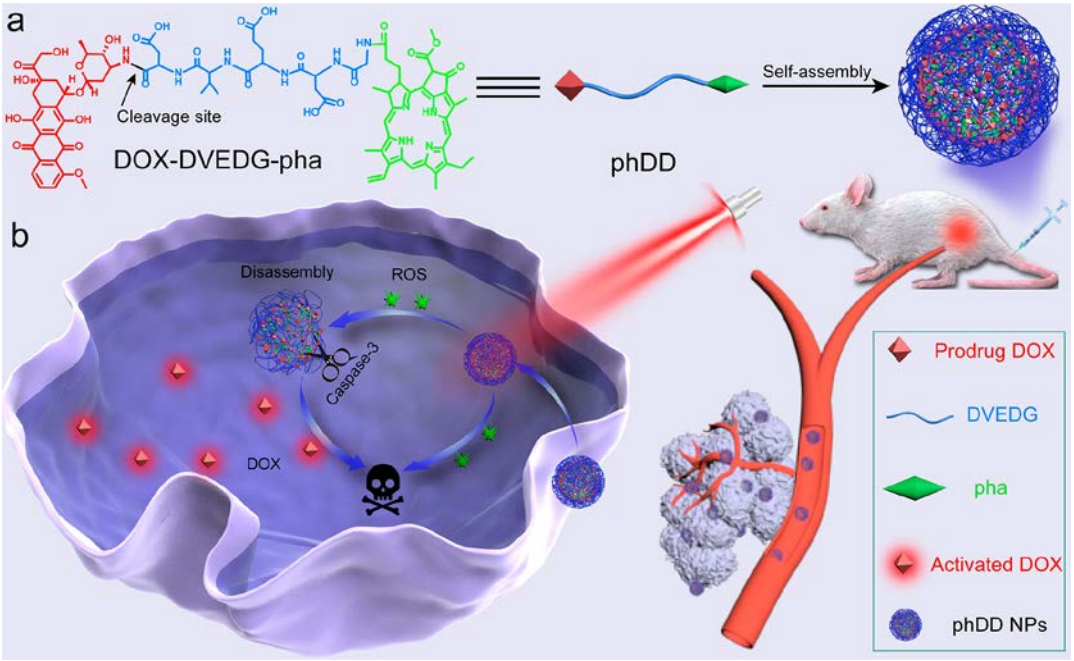

s1 therapy. As shown in Scheme 1a, the phDD molecules can self-assemble into spherical nanoparticles under physiological conditions. After injecting into mice through the tail vein, it can be enriched to tumor sites through the EPR effect (Scheme 1b).[20] Upon the light irradiation, the photosensitizer (pha) would produce ROS to initiate the cell apoptosis process and further activate the caspase-3 enzyme. Furthermore, the activated caspase-3 enzyme could cleave the peptide sequences specifically to release the DOX, which would cause the subsequent chemotherapy in the tumor site, as expressed in Scheme 1b. At the same time, the systemic toxicity caused by immature leakage could be avoided due to the caspase-3 response process that only occurred in the presence of light.

EXPERIMENTAL SECTION

Materials. 2-Chlorotrityl chlorideresin, Fmoc-protected L-amino acids, and HBTU were both obtained via GL Shanghai Biochem Ltd. (China). Diisopropylethylamine (DIPEA) and piperidine were gained through GL Biochem Ltd. Doxorubicin hydrochloride (DOX·HCl) was purchased from Macklin Biochemical Co., Ltd. (Shanghai, China). Dulbecco's modified Eagle's medium (DMEM), fetal bovine serum (FBS), trypsin, MTT, penicillin, and streptomycin were all gained from GIBCO Invitrogen Corp. The pheophorbide-a (pha) was obtained by 271 Frontier Scientific (Logan, UT, USA). 2′,7′-Dichlorodihydrofluorescein diacetate (DCFH-DA) was provided through Sigma-273 Aldrich (USA). The caspase-3 enzyme was purchased from R&D systems 272 (USA). Triisopropylsilane (TIS) and trifluoroacetic acid (TFA) were purchased by Shanghai Reagent Chemical Co. (Shanghai, China).

Synthesis of phD, phDD, and phED. phD (HOOC-Asp(otBu)-Val-Glu(otBu)-Asp(otBu)-Gly-pha) was prepared as in our previous report.[21] The 2-chlorotrityl chlorideresin was swollen using anhydrous DMF as the solution for about 60 min in nitrogen atmosphere. Fmoc group deprotection was performed using 20% piperidine in DMF at room temperature for 20 min. HBTU/DIPEA was used as the coupling agent to connect amino acids to the peptide on the resin sequentially. The phD was collected using the cleavage solution (TFA:TIS:H_2O = 95:2.5:2.5) which was cleaved from the resin for 90 min. Then, we precipitated this final solution into diethyl ether, centrifuged, and put it into a vacuum for one night to get the crude product. phDD (DOX-DVEDG-pha) was conjugated with doxorubicin hydrochloride (1.2-fold excess of phD) in anhydrous DMF using DIPEA and HBTU (1.5-fold excess of phD) as the coupling agents, where TEA was added to react with the HCl in DOX·HCl. The reaction mixture was dialyzed using a MWCO 500 membrane against deionized water and anhydrous DMF (1:1) several times in room temperature until the solution was totally colorless and lyophilized overnight. The protecting group of phDD was cleaved just the same as the phD. Then, we precipitated the phDD into diethyl ether, centrifuged, and put it into a vacuum for one night to get the crude product. The purity and the molecular weight of phDD were analyzed by high-performance liquid chromatography (HPLC) and ESI-MS, respectively. HPLC was performed using a Gemini-NX 10 μC18 100A column (4.6 × 250 mm) with acetonitrile (0.1% of TFA) and water (0.1% of TFA) as the eluent. The gradient was: 0−0.01 min 10% acetonitrile and 90% water; 0.01−35 min 90% acetonitrile and 10% water; 35.01−40 min 100% acetonitrile. As a control, the phED (DOX-VDEDG-pha) was obtained by a similar method.

Characterizations of phDD. UV−vis absorption spectra were acquired via a Nicolet Evolution 300 UV−vis spectrometer (Thermo Nicolet, USA). Fluorescence spectra were obtained by analyzing a fluorophotometer (RF-5301 PC, Japan) (excitation wavelength: 405 nm (pha) and 475 nm (DOX·HCl), emission wavelength: 600−750 nm and 500−650 nm). After phDD was dissolved in PBS buffer (25 μg mL^{-1}), the dynamic light scattering was measured by Nano-ZS ZEN3600 (Malvern Instruments, UK) at room temperature. The morphology of phDD was examined by TEM (JEM-2100 microscope, Japan).

Reactive Oxygen Species (ROS) Detection. An amount of 30 μL of DCFH-DA (1 μg mL^{-1}, pretreated with NaOH) was mixed with 970 μL of phDD solution with different treatments and the fluorescence intensity at intervals of 5 s using white light (excitation wavelength = 488 nm, emission wavelength = 525 nm), PBS, and pha (dissolved in PBS) as the control. The ROS generation ability was calculated by F_t/F_0 (F_0: the starting fluorescence; F_t: the fluorescence of samples with various times).

https://dx.doi.org/10.1021/acsabm.0c00122
ACS Appl. Bio Mater. XXXX, XXX, XXX−XXX

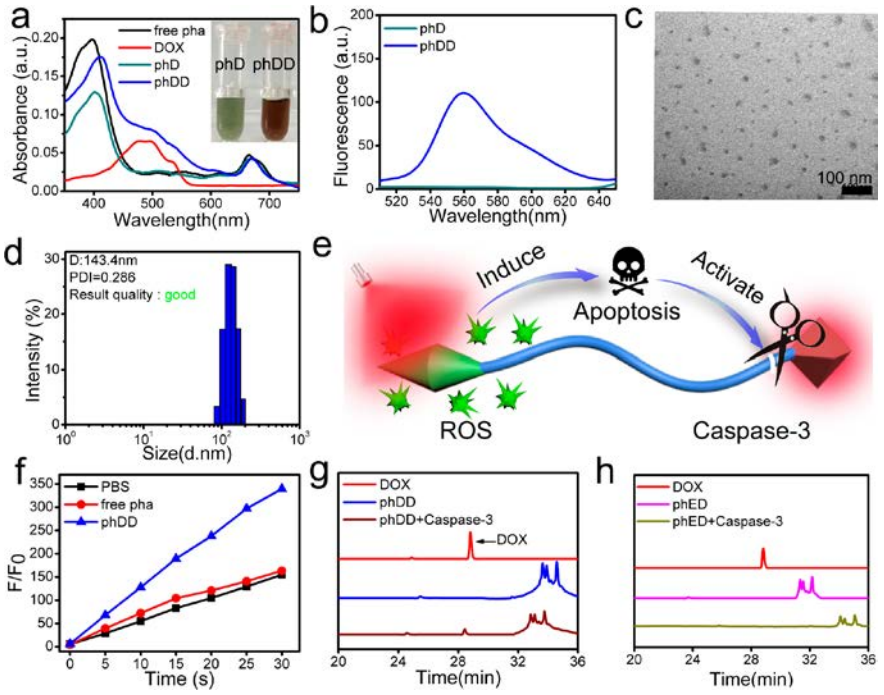

Figure 1. (a) UV−vis spectra of free pha (black), DOX (red), phD (dark cyan), and phDD nanoparticles (blue). (b) Fluorescence spectrum of phD (dark cyan) and phDD (blue). (c) TEM image and (d) hydrodynamic size of phDD solution. (e) Schematic diagram of phDD nanoparticles producing ROS and inducing release of DOX under light irradiation. (f) ROS generation of PBS (black), free pha (red), and phDD (blue) under light irradiation using DCFH-DA as the sensor. (g) HPLC traces of DOX (red), free phDD (blue), and phDD incubated with caspase-3 for 24 h (wine). (h) HPLC traces of DOX (red), free phED (pink), and phED incubated with caspase-3 for 24 h (olive).

High Performance Liquid Chromatography. The phED and phDD (80 μg mL^{-1}) were incubated with caspase-3 (5 ng mL^{-1}) in the reaction buffer (50 mM HEPES, 10 mM dithiothreitol, 0.1% CHAPS, 100 mM NaCl, and 1 mM EDTA, pH 7.5) in 37 °C. After 24 h, samples were diluted and characterized by reversed-phase high performance liquid chromatography (RP-HPLC) (Waters XBridge-C18 column). A 5 μL sample was injected on a C18 column equilibrated with a methanol/water (5/95 v/v) mobile phase which contains 0.1% trifluoroacetic acid (TFA). The sample was separated by a linear increase of the methanol concentration by 5% to 100% for 35 min at a flow rate of 1.5 mL/min. The RP-HPLC profile was monitored at a wavelength of 400 nm.

Western Blot Analysis. 4T1 cells were seeded in the 6-well plates, and then various samples were added into the different plates when the cells grew to about 70%. About 4 h later, plates were washed with PBS and replaced with fresh DMEM. After that, the plates received light irradiation (633 nm, 50s). After 24 h, the samples were executed to prepare for the standard Western blot procedure.

Cell Viability Assay. The cytotoxicity of phD, phED, and phDD against 4T1 cells was determined by an MTT assay. 4T1 cells were seeded in the 96-well plates, and when the cells grew up to 60−80% in the fields, a series of concentrations of phD, phDD, or phED were added into the plates. After 4 h incubation, the materials were removed and replaced with 100 μL of DMEM in each hole. The plates received the light irradiation (phDD: 30 s, phED and phDD: 30 s, 10 mW cm^{-2}). Subsequently, the plates were incubated for 1 day. An amount of 20 μL of MTT in each well (5 mg mL^{-1}) was added. After 4 h, the above solution was replaced with 150 μL of DMSO per well. The optical density (OD) values at 490 nm were recorded by a microplate reader. The relative cell viability was also calculated by the following formula: cell viability (%) = $OD_{(sample)}/OD_{(control)} \times 100\%$, where $OD_{(sample)}$ was the OD value in the presence of sample and $OD_{(control)}$ was the optical density in the absence of the sample.

Colocalization and Separation of Doxorubicin by CLSM. 4T1 cells were added into the plates. After 24 h, phED, phDD (50 μg mL^{-1}), and DOX·HCl (18 μg mL^{-1}) were incubated with cells. After 4 h, materials were replaced with DMEM. Hochest 33342 was used for labeling the nuclei. Then, the plates were washed by PBS for three times. Cell images were photographed using the CLSM.

Calcein AM/PI and Annexin V-FITC/PI Staining. 4T1 cells were added into the plates. Subsequently, phED, phDD, and DOX·HCl were incubated with the various plates. After 3 h, the solutions were replaced with PBS buffer, and the fresh DMEM was added. The plates were irradiated with light (633 nm, 60s). After 2 h, the cells were stained with Calcein AM (1×10^{-6} M) and PI (4.5×10^{-6} M). The images of samples were shot via CLSM (Leica TCS SP8, German) 30 min later.

For the flow cytometry, first, 4T1 cells were seeded in the plates. When the cells were growing up to 60−80%, PBS, phED, phDD, and doxorubicin were added. After 4 h, the samples were removed and replaced with fresh DMEM, and then the plates were irradiated for 20 s. After 12 h, the cells were digested, collected, and stained with Annexin V-FITC/PI in the tubes for about 25 min at room temperature. Finally, the tubes of various samples were tested.

Pharmacokinetics, Animal Imaging, and Tissue Distributions. All animal experiments were executed based on the 4T1 tumor-bearing mice (6−8 weeks female BALB/c mice) according to the criteria of The National Regulation of China. For pharmacokinetics study, phDD was injected into 4T1 tumor-bearing mice (200 μL, 1 mg mL^{-1}). An amount of 10 μL of blood was collected each time through the tail vein. PBS was added into the samples, and the final volume is 100 μL. To disrupt the cell, they were freeze−thawed several times, and then the samples were received 30 min sonication. Subsequently, they were centrifuged (3000 r/min) for 5 min and took out the supernatant to measure the amount of pha using the fluorescence spectrum.

For animal imaging and tissue distributions, the mice were injected into phDD nanomaterials (250 μL, 400 μg mL^{-1}) by a tail vein. At the present time, these results of animal imaging were performed utilizing a small animal imaging system. After 24 h, the organs and tumor were flaked from the mice and imaged.

Antitumor Therapy and Systematic Toxicity *in Vivo*. An amount of 5×10^6 of 4T1 cells was seeded subcutaneously into the female mice. After the tumor model was established, they were

https://dx.doi.org/10.1021/acsabm.0c00122
ACS Appl. Bio Mater. XXXX, XXX, XXX−XXX

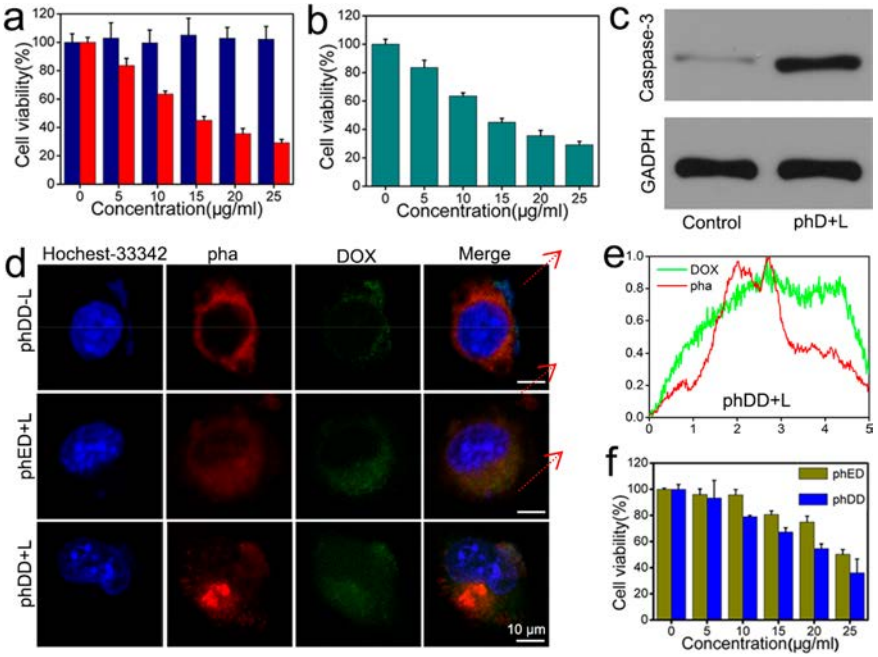

Figure 2. (a) Cell viability of DOX (red) and phDD nanoparticles (navy) in the dark. (b) Cell viability of phDD (dark cyan) under light irradiation for 30 s (633 nm, 10 mW cm^{-2}). (c) Western blots of caspase-3 treated with phD + L under light irradiation for 50 s (633 nm, 10 mW cm^{-2}). (d) CLSM images and (e) line scan results of 4T1 cells after incubation with various samples (phDD-L, phED + L, phDD + L). (f) Cell viability of phED (dark yellow) and phDD (blue) under light irradiation for 30 s (633 nm, 10 mW cm^{-2}).

divided into five groups randomly. For the doxorubicin group, 42 μL of doxorubicin solution (500 μg mL^{-1} dissolved in pure water) was injected via the abdominal cavity. For phDD and phED groups, 120 μL of solution was injected into the mice through the tail vein (500 μg mL^{-1}). After 4 h, the mice received 5 min laser irradiation (682 nm, 0.2 mW cm^{-2}). The volume of the tumor and the weight of mice were recorded each day. The size was calculated according to eq 1, where a and b stand for the length and width of the tumor, respectively. Fourteen days later, all of the tumors were exfoliated, weighted, and photographed. The whole blood was collected for blood analysis and blood biochemical examination.

$$V\ (\mathrm{mm}^3) = \frac{a \times b^2}{2} \quad (1)$$

For histological observation, the various organs and tumors were collected and added into 4% formalin after the mice were sacrificed. Subsequently, the various samples were embedded in paraffin. They were sent to Wuhan baiqiandu Biological Technology Co., Ltd. for H&E and immunocytochemistry testing.

RESULTS AND DISCUSSION

Synthesis, Characterization, and Photoactivity Properties of phDD Nanoparticles. phDD was synthesized through the solid-phase peptide synthesis (SPPS) method (Scheme S1).[22] According to Figures S1−S3, the ESI-MS of products 1, 2, and 3 (phDD) were shown, respectively, which demonstrated that the products 1, 2, and 3 were successfully synthesized and had high purity. At the same time, only a single peak of phDD can be observed by HPLC, which means that high-purity phDD was obtained (Figure S4). As shown in Figure 1a, there was a clear UV−vis absorption spectrum at 500 nm in the phDD solution, which indicated that DOX was grafted into the peptide. This conclusion can also be drawn from the color change of the solution in the inset of Figure 1a. At the same time, the UV−vis spectra of phD and phDD showed that the pha structure in both was in a well-dispersed state with a slight blue shift at 667 nm (Figure 1a).[23,24] The free pha showed two broad peaks around 667 and 685 nm, which indicated that the pha wAs aggregated. The difference was caused by the hydrophobic interaction or $\pi-\pi$ stacking between pha molecules. After pha were modified with the DEVD peptide, the carboxyl could reduce the aggregation between pha molecules and improve the stability. What's more, the fluorescence characteristic peaks of DOX can be detected in phDD solution, indicating that DOX was successfully coupled with phD (Figures 1b and S5). Transmission electron microscopy (TEM) results suggested that the phDD nanoparticles had reasonable size and good dispersibility (Figure 1c). The dynamic light-scattering (DLS) results showed the size of phDD nanoparticles was 143 nm (Figure 1d), and the low PDI (0.286) suggested the good dispersibility. There may exist a discrepancy between TEM and DLS results, as the nanoparticles could shrink in the vacuum state.

To evaluate the reactive oxygen species (ROS) generation efficiency of the phDD, the ROS test experiments were performed using 2′,7′-dichlorodifluorescein diacetate (DCFH-DA) as the fluorescence probe. As we all know, the DCFH-DA could be oxidized and turned into green fluorescence DCF when it came across the ROS.[25,26] The amount of ROS depends upon the radical intermediates which can be produced via the irradiated photosensitizer. The phDD nanoparticles had high production efficiency of ROS, which can effectively induce apoptosis and further activate the caspase-3 enzyme. The activated caspase-3 enzyme would recognize the DEVD sequence in the peptide phDD, thereby selectively releasing prodrugs through caspase-3 in response to the specific sequence (Figure 1e).[27−29] According to Figure 1f, compared with the fluorescence intensity of the free pha (dissolved in DMSO and dispersed in PBS) and the PBS group, the ROS fluorescence intensity of the phDD group increased significantly over time, faster than that of the control group. The reason was that the pha structure in phDD nanoparticles

https://dx.doi.org/10.1021/acsabm.0c00122
ACS Appl. Bio Mater. XXXX, XXX, XXX−XXX

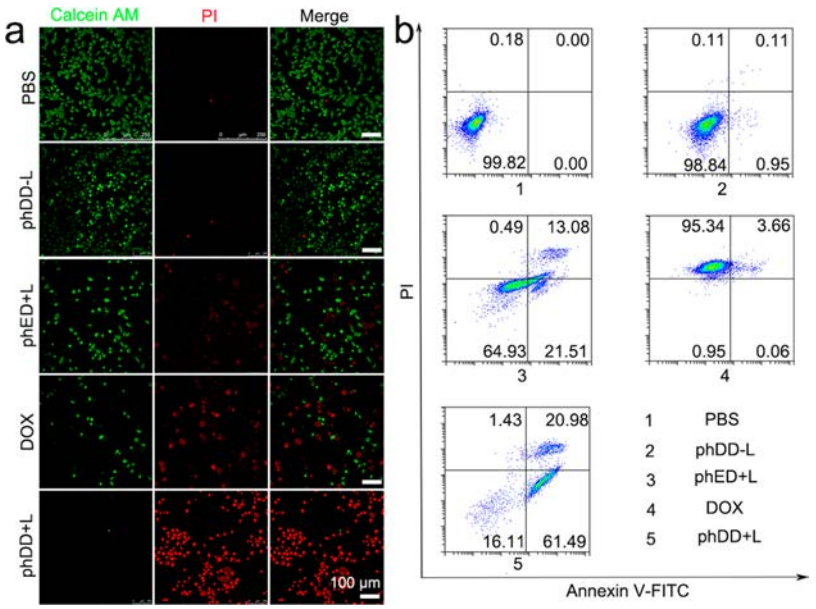

Figure 3. (a) Calcein AM/PI staining and (b) flow cytometry analysis of the 4T1 cell after incubation with various samples (PBS, phDD − L, phED + L, DOX, and aphDD + L). Scale bar: 100 μm.

remained stable and dispersive, while the free pha aggregated due to $\pi-\pi$ accumulation. Next, HPLC was performed to confirm that the caspase-3 could release DOX from the phDD nanoparticles. When phDD nanoparticles and caspase-3 were incubated together for 24 h, there was a distinctive DOX characteristic peak with a retention time consistent with the standard. However, after the same treatment of phED nanoparticles, no DOX characteristic peak was observed. DOX was also not detected in both free phDD and phED (Figure 1g and 1h). These results indicated that phDD nanoparticles can successfully respond to the caspase-3 enzyme after a series of treatments and then release the prodrug smoothly.

Efficient Photodynamic and Combined Chemotherapy with Low Side Effects *in Vitro*. Considering the good dispersity of phDD nanoparticles, the ROS generation ability, and the caspase-3-responsive property, a series of cell viability experiments were continued to execute to test its biocompatibility and selectivity. Here, the methyl thiazolyl tetrazolium (MTT) assay was used to verify this suspicion. As shown in Figure 2a, 4T1 cells were incubated with phDD nanoparticles and DOX in the dark, respectively. It was obvious that phDD nanoparticles had no toxicity without light irradiation. However, the toxicity was much higher than that of phDD nanoparticles when DOX was incubated with the cells. The results demonstrated that DOX can kill cells at will, but phDD nanoparticles can prevent the release of prodrugs to kill cells in dark conditions, indicating its potential for low toxicity. Next, phDD nanoparticles were used to study apoptosis under light. As can be seen from Figure 2b, cell viability depended on the concentration of phDD nanoparticles. When the final concentration reached 25 μg mL^{-1}, the cell viability was reduced to about 30%, which indicated that phDD nanoparticles had strong cytotoxicity and good photodynamic effect when exposed to light. Soon, the feasibility of Western blots of caspase-3 were continued to be evaluated after phD was exposed to light for 50 s (633 nm, 10 mW cm^{-2}). Figure 2c showed that the phD could efficiently activate caspase-3 enzyme under the light irradiation. The release of prodrugs that can specifically respond to light can be further verified by confocal laser scanning microscopy (CLSM). After incubating cells with various samples, it was clearly shown that the fluorescence between DOX and pha was well colocalized in cells treated with phDD-L and phED + L (Figure 2d) and had fluorescence overlap, respectively (Figures S6a and S6b). However, it can be seen from Figures 2d and 2e that phDD + L-treated cells had a clear fluorescence separation of green (DOX) and red (pha) light, and the released DOX can enter the nucleus only after being treated by the phDD + L group. All these results indicated that caspase-3 was able to successfully cleave the response peptide sequence. Most importantly, after cell incubation with phDD and phED under light conditions, the cytotoxicity of the phED group was significantly lower than that of the phDD group (Figure 2f). All these results indicated that phDD can selectively release DOX to complete adjuvant therapy.

Excited by the above excellent results, the synergistic therapy based on the apoptosis behaviors was investigated via the CLSM. Calcein AM and pyridine iodide (PI) were employed here to evaluate the potential ability of various samples to kill tumor cells because the red and green fluorescence could reflect the percentage of cell viability. As shown in Figure 3a, the red fluorescence intensity of the phDD + L group was higher than that of the other groups, indicating that the cells died to the greatest extent. Especially in the phDD − L group, such a huge difference was caused simply by the lighting conditions. Although the phED + L group and the DOX group showed mild red fluorescence, these phenomena indicated that phDD + L had good ROS production efficiency and can effectively release doxorubicin under light irradiation to achieve the purpose of combined therapy. Subsequently, the flow cytometry was performed to further verify this result. According to Figure 3b, cells treated with phDD − L exhibited the good survival behavior, and the cells treated with free DOX resulted in more than 90% apoptotic cells, which indicated that the phDD had outstanding biocompatibility. Cells treated with phED + L resulted in 21.5% early apoptotic and 13% late apoptotic cells. However, phDD + L treated cells showed a

https://dx.doi.org/10.1021/acsabm.0c00122
ACS Appl. Bio Mater. XXXX, XXX, XXX−XXX

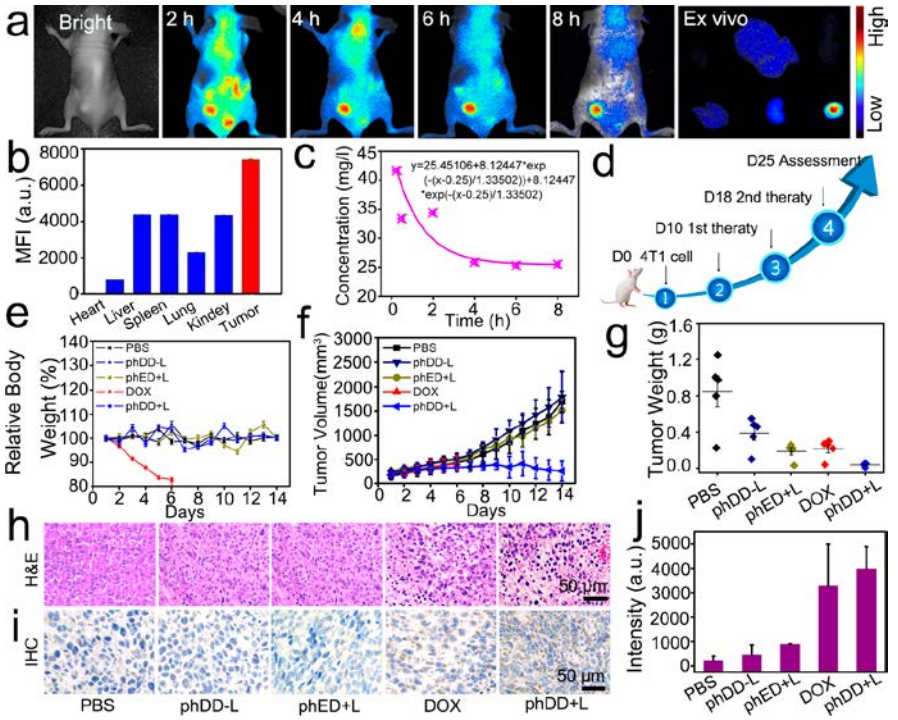

Figure 4. (a) Fluorescence imaging of phDD in the tumor site (red circle) at different time points (2 h, 4 h, 6 h, 8 h) and fluorescence imaging of the main organs and tumors after tail vein injection for 24 h. (b) The mean fluorescence intensity of organs and tumor. (c) Pharmacokinetics of phDD after intravenous injection (pha as the fluorescence reference). (d) The workflow of animal therapy experiments and assessment. (e) Relative body weight changes in mice receiving different treatments. (f) After different treatments on the 3rd and 11th days, the tumor volume changed daily within 14 days. (g) Distribution of tumor weight after euthanasia of mice. (h) H&E staining of tumors treated by different therapies. Scale bars: 50 μm. (i) Immunohistochemical staining of caspase-3 in tumor tissues after different therapies. Scale bars: 37.5 μm. (j) The quantitative intensity of caspase-3 expression.

higher percentage of apoptotic behavior, which was up to 61% early apoptotic cells and 20% late apoptotic cells, respectively. The PBS group showed the lowest percentage of apoptosis. The CLSM and flow cytometry (Figure 3) results all indicated that the combined therapy of photodynamic therapy and chemotherapy was selectively activated by light and had an excellent outcome.

High Tumor Targeting and Antitumor Therapy Studies *in Vivo*. Subsequently, tumor targeting of phDD was monitored by small animal imaging system. After the 4T1 tumor-bearing nude mouse was intravenously injected with phDD, the mouse was imaged at an interval of 2 h. As shown in Figure 4a, the fluorescence imaging was gradually enhanced, reached a maximum at 4 h, and remained stable after 6 h. After 8 h, there was almost no fluorescence in the body of the mouse, while the fluorescence in the tumor site kept steady, which indicated the good tumor targeting of phDD. The good targeting ability of phDD nanoparticles in the tumor resulted from the carboxyl groups in phDD. The carboxylate radical could be rapidly protonated to neutral carboxylic acid [COOH] at the tumor extracellular acidic microenvironment, which increased the hydrophobicity of phDD and drove the internalization of phDD, resulting in higher tumor accumulation.[30,31] After 24 h, the mice were euthanized, and the major organs and tumors were imaged. It was found that the drug can be retained in the tumor tissue for a long time. The semiquantitative calculation of the mean fluorescence intensity (MFI) values showed that the MFI at the tumor was higher than the MFI of organs, even twice as high as the MFI of the main metabolic organs (kidney, liver, and spleen) (Figure 4b). This result was also significantly higher than our previous works (Zhang et al.) about tumor-targeted delivery.[32,33] The pharmacokinetics in Figure 4c indicated that phDD could quite steadily stay in the blood. All these results showed the phDD had an outstanding tumor targeting ability and stability.

Next, the antitumor efficiency of photodynamic and chemo combined therapy was executed. The mice were divided into five groups (PBS, phDD − L, phED + L, DOX, phDD + L). All mice were inoculated with 4T1 tumor cells. After 7 days of growth, the average tumor volume reached 206 ± 71 mm^3. When the tumor model was established, the treatment was performed according to the experimental procedure of Figure 4d. The corresponding treatments were performed on the 10th and 18th days, respectively. The therapeutic effect of the mice was evaluated on the 25th day. Meanwhile, the tumor volume and body weight were measured each day during the therapy. According to Figure 4e, the mice body weight almost kept steady, except for the DOX group, and the mice of the DOX group only survived 6 days after performing the therapy, as the DOX caused severe toxicity. On the other hand, the other groups all survived during this process. The above results indicated that the phDD had high biocompatibility without the light, while DOX had strong systematic toxicity, as it is nontargeting. Next, the tumor volume of various samples was measured as Figure 4f shows. PhDD + L-treated mice showed the most enhanced antitumor efficiency. Based on the differences of volume, the phDD+L group was 206 ± 202 mm^3. There may exist the diffusion of the activated DOX into the adjacent tumor site to cause the sequential events.[34] However, the PBS group even grew up to 1690 ± 216 mm^3 in

https://dx.doi.org/10.1021/acsabm.0c00122
ACS Appl. Bio Mater. XXXX, XXX, XXX−XXX

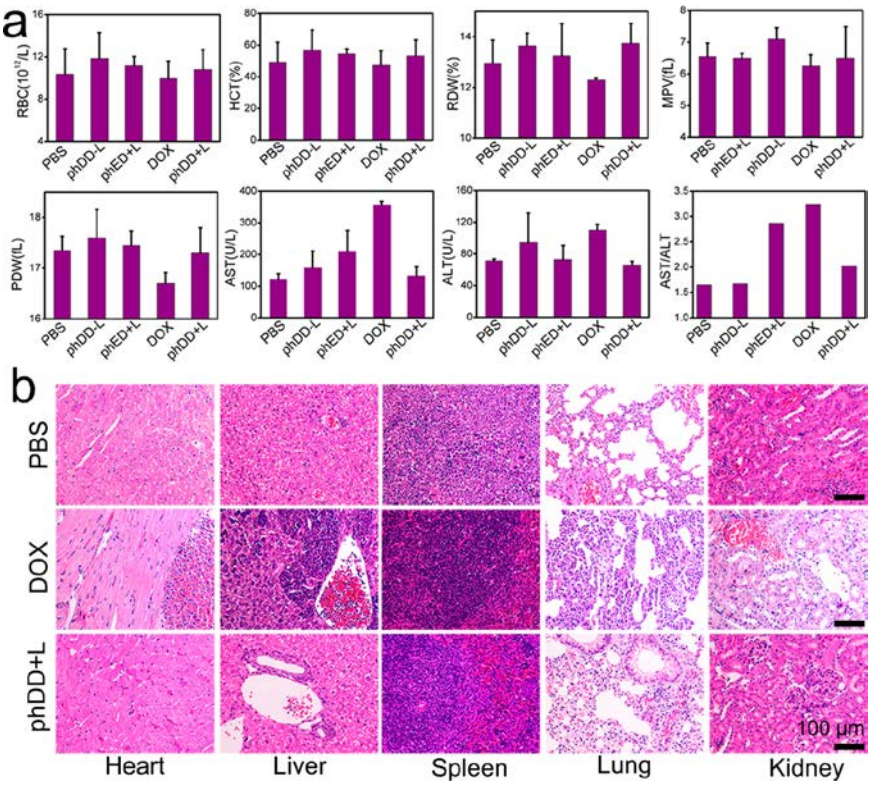

Figure 5. (a) Whole blood tests and biochemical blood indicators of mice treated with various samples. (b) The H&E staining of main organs after mice treated with various samples.

the last day, which was eight times more than the volume of the phDD + L group. The mice were sacrificed, and the main organs and tumor were gained after 14 days' treatment. According to Figures 4g and S7, the tumor weight and photographs indicated that phDD could effectively kill tumor cells, while other groups were unsatisfactory. What's more, H&E staining and immunohistochemical (IHC) analyses were adopted to evaluate the therapy outcome. Hematoxylin-eosin (H&E) staining (Figure 4h) gave the apparent evidence that there existed severe cell death in the tumor treated with the phDD + L group compared to the PBS and other groups, and the IHC analyses (Figure 4i) also confirmed there existed an increase of caspase-3 enzyme in the tumor site treated with the phDD + L group. While the PBS group showed little caspase-3 expression, the DOX group showed a slight increase of caspase-3. The quantitative of IHC analyses also clearly indicated the enhanced caspase-3 expression treated with phDD + L (Figure 4j), which was because of the outstanding combined therapy.

Systematic Toxicity Analysis. Finally, the complete blood panel test and blood biochemical examination were conducted to verify the systemic toxicity. As Figure 5a showed, all the parameters treated with free DOX of blood panel were slightly lower than other groups, while the group of phDD + L had no significant difference compared to the PBS and others. The blood biochemical examination results of free DOX were significantly higher than the PBS and phDD + L group, which indicated the potential systemic toxicity of free DOX. The main organs of H&E staining also demonstrated that there existed severe damage treated with free DOX. Due to the slight congestion in the heart, there was a slight decrease in cellularity in the spleen, change in cellularityn, and crowded nuclei in the liver, which may suggest tumor metastasis (Figures 5b and S8). All these above results demonstrated that phDD could protect the prodrug from killing normal cells, and the controllable light could activate the release of DOX. Free DOX had the enhanced systematic toxicity. This method of light-responsive prodrug was meaningful in clinical therapy.

CONCLUSIONS

In summary, a photosensitizer−drug conjugate that responds to a series of light-induced cascade events can be selectively activated at the tumor site for low side effect drug release and effective combination therapy. This conjugate could self-assemble into the spherical nanoparticle under physiological conditions and efficiently target the tumor site. Upon the controlled light irradiation, the phDD nanoparticles could activate caspase-3 and subsequently prodrugs. This strategy could significantly reduce the systemic toxicity without impairing the PDT efficiency. Both *in vitro* and *in vivo* results demonstrated the suppression of tumor growth with ultralow systemic toxicity. This research could solve the unavoidable systemic toxicity and inefficient PDT chemotherapy in traditional drug delivery systems (DDSs), which can give a promising approach for controllable drug activation and more effective PDT/chemo combination therapy.

ASSOCIATED CONTENT

Supporting Information

The Supporting Information is available free of charge at https://pubs.acs.org/doi/10.1021/acsabm.0c00122.

Scheme of phDD synthesis; HPLC and ESI-MS of phDD; fluorescence spectrum of phD and phDD; CLSM line scan images of phDD − L and phED + L group; photograph of tumor treated with various

https://dx.doi.org/10.1021/acsabm.0c00122
ACS Appl. Bio Mater. XXXX, XXX, XXX−XXX

samples; H&E staining of phDD − L and phED + L group (PDF)

AUTHOR INFORMATION

Corresponding Author

He-You Han − *State Key Laboratory of Agricultural Microbiology, College of Science and State Key Laboratory of Agricultural Microbiology, College of Life Science and Technology, Huazhong Agricultural University, Wuhan 430070, China*; orcid.org/0000-0001-9406-0722; Email: hyhan@mail.hzau.edu.cn

Authors

Yong-Li Mu − *State Key Laboratory of Agricultural Microbiology, College of Science, Huazhong Agricultural University, Wuhan 430070, China*

Jin Zhang − *State Key Laboratory of Agricultural Microbiology, College of Life Science and Technology, Huazhong Agricultural University, Wuhan 430070, China*

Meng-Qing Xu − *State Key Laboratory of Agricultural Microbiology, College of Science, Huazhong Agricultural University, Wuhan 430070, China*

Mohamed F. Foda − *State Key Laboratory of Agricultural Microbiology, College of Science and State Key Laboratory of Agricultural Microbiology, College of Life Science and Technology, Huazhong Agricultural University, Wuhan 430070, China; Department of Biochemistry, Faculty of Agriculture, Benha University, Moshtohor, Toukh 13736, Egypt*; orcid.org/0000-0002-2672-1370

Yang Wu − *State Key Laboratory of Agricultural Microbiology, College of Life Science and Technology, Huazhong Agricultural University, Wuhan 430070, China*

Complete contact information is available at: https://pubs.acs.org/10.1021/acsabm.0c00122

Author Contributions

#Y.L.M. and J.Z. contributed equally.

Notes

The authors declare no competing financial interest.

ACKNOWLEDGMENTS

This work was financially supported by the National Natural Science Foundation of China (21778020, 31750110464, 31950410755) and Sci-tech Innovation Foundation of Huazhong Agriculture University (2662017PY042, 2662018PY024).

REFERENCES

(1) Chen, Z. Small-Molecule Delivery by Nanoparticles for Anticancer Therapy. *Trends Mol. Med.* **2010**, *16*, 594−602.

(2) Meng, L.; Zhang, X.; Lu, Q.; Fei, Z.; Dyson, P. J. Single Walled Carbon Nanotubes as Drug Delivery Vehicles: Targeting Doxorubicin to Tumors. *Biomaterials* **2012**, *33*, 1689−1698.

(3) Torchilin, V. P.; Lukyanov, A. N. Peptide and Protein Drug Delivery to and into Tumors: Challenges and Solutions. *Drug Discovery Today* **2003**, *8*, 259−266.

(4) Duncan, R. The Dawning Era of Polymer Therapeutics. *Nat. Rev. Drug Discovery* **2003**, *2*, 347−360.

(5) Murakami, T.; Tsuchida, K. Recent Advances in Inorganic Nanoparticle-Based Drug Dlivery Systems. *Mini-Rev. Med. Chem.* **2008**, *8*, 175−183.

(6) Zheng, M.; Yue, C.; Ma, Y.; Gong, P.; Zhao, P.; Zheng, C.; Sheng, Z.; Zhang, P.; Wang, Z.; Cai, L. Single-Step Assembly of DOX/ICG Loaded Lipid-Polymer Nanoparticles for Highly Effective Chemo-Photothermal Combination Therapy. *ACS Nano* **2013**, *7*, 2056−2067.

(7) Wang, K.; Hu, Q.; Zhu, W.; Zhao, M.; Ping, Y.; Tang, G. Structure-Invertible Nanoparticles for Triggered Co-Delivery of Nucleic Acids and Hydrophobic Drugs for Combination Cancer Therapy. *Adv. Funct. Mater.* **2015**, *25*, 3380−3392.

(8) Popat, A.; Ross, B. P.; Liu, J.; Jambhrunkar, S.; Kleitz, F.; Qiao, S. Z. Enzyme-Responsive Controlled Release of Covalently Bound Prodrug from Functional Mesoporous Silica Nanospheres. *Angew. Chem., Int. Ed.* **2012**, *51*, 12486−12489.

(9) Xu, Z.; Liu, S.; Kang, Y.; Wang, M. Glutathione-and pH-Responsive Nonporous Silica Prodrug Nanoparticles for Controlled Release and Cancer Therapy. *Nanoscale* **2015**, *7*, 5859−5868.

(10) Kong, F.; Liang, Z.; Luan, D.; Liu, X.; Xu, K.; Tang, B. A Glutathione (GSH)-Responsive Near-Infrared (NIR) Theranostic Prodrug for Cancer Therapy and Imaging. *Anal. Chem.* **2016**, *88*, 6450−6456.

(11) Feng, L.; Cheng, L.; Dong, Z.; Tao, D.; Barnhart, T. E.; Cai, W.; Chen, M.; Liu, Z. Theranostic Liposomes with Hypoxia-Activated Prodrug to Effectively Destruct Hypoxic Tumors Post-Photodynamic Therapy. *ACS Nano* **2017**, *11*, 927−937.

(12) Li, Z.; Wang, H.; Chen, Y.; Wang, Y.; Li, H.; Han, H.; Chen, T.; Jin, Q.; Ji, J. pH-and NIR Light-Responsive Polymeric Prodrug Micelles for Hyperthermia-Assisted Site-Specific Chemotherapy to Reverse Drug Resistance in Cancer Treatment. *Small* **2016**, *12*, 2731−2740.

(13) Min, Y.; Li, J.; Liu, F.; Yeow, E. K.; Xing, B. Near-Infrared Light-Mediated Photoactivation of A Platinum Antitumor Prodrug and Simultaneous Cellular Apoptosis Imaging by Upconversion-Luminescent Nanoparticles. *Angew. Chem., Int. Ed.* **2014**, *53*, 1012−1016.

(14) Olejniczak, J.; Carling, C.-J.; Almutairi, A. Photocontrolled Release Using One-Photon Absorption of Visible or NIR Light. *J. Controlled Release* **2015**, *219*, 18−30.

(15) Yuan, Y.; Min, Y.; Hu, Q.; Xing, B.; Liu, B. NIR Photoregulated Chemo-and Photodynamic Cancer Therapy Based on Conjugated Polyelectrolyte-Drug Conjugate Encapsulated Upconversion Nanoparticles. *Nanoscale* **2014**, *6*, 11259−11272.

(16) Liu, C.; Zhang, Y.; Liu, M.; Chen, Z.; Lin, Y.; Li, W.; Cao, F.; Liu, Z.; Ren, J.; Qu, X. A NIR-Controlled Cage Mimicking System for Hydrophobic Drug Mediated Cancer Therapy. *Biomaterials* **2017**, *139*, 151−162.

(17) Tian, Y.; Zheng, J.; Tang, X.; Ren, Q.; Wang, Y.; Yang, W. Near-Infrared Light-Responsive Nanogels with Diselenide-Cross-Linkers for On-Demand Degradation and Triggered Drug Release. *Part. Part. Syst. Char.* **2015**, *32*, 547−551.

(18) Li, F.; Li, T.; Cao, W.; Wang, L.; Xu, H. Near-Infrared Light Stimuli-Responsive Synergistic Therapy Nanoplatforms Based on the Coordination of Tellurium-Containing Block Polymer and Cisplatin for Cancer Treatment. *Biomaterials* **2017**, *133*, 208−218.

(19) Wang, Y.; Deng, Y.; Luo, H.; Zhu, A.; Ke, H.; Yang, H.; Chen, H. Light-Responsive Nanoparticles for Highly Efficient Cytoplasmic Delivery of Anticancer Agents. *ACS Nano* **2017**, *11*, 12134−12144.

(20) Maeda, H. Toward a Full Understanding of the EPR Effect in Primary and Metastatic Tumors as Well as Issues Related to Its Heterogeneity. *Adv. Drug Delivery Rev.* **2015**, *91*, 3−6.

(21) Zhang, J.; Mu, Y.-L.; Ma, Z.-Y.; Han, K.; Han, H.-Y. Tumor-Triggered Transformation of Chimeric Peptide for Dual-Stage-Amplified Magnetic Resonance Imaging and Precise Photodynamic Therapy. *Biomaterials* **2018**, *182*, 269−278.

(22) Liu, L. H.; Qiu, W. X.; Zhang, Y. H.; Li, B.; Zhang, C.; Gao, F.; Zhang, L.; Zhang, X. Z. A Charge Reversible Self-Delivery Chimeric Peptide with Cell Membrane-Targeting Properties for Enhanced Photodynamic Therapy. *Adv. Funct. Mater.* **2017**, *27*, 1700220.

(23) Eichwurzel, I.; Stiel, H.; Röder, B. Photophysical Studies of the Pheophorbide a Dimer. *J. Photochem. Photobiol., B* **2000**, *54*, 194−200.

(24) Zhang, J.; Xu, M.; Mu, Y.; Li, J.; Foda, M. F.; Zhang, W.; Han, K.; Han, H. Reasonably Retard O2 Consumption Through A Photoactivity Conversion Nanocomposite for Oxygenated Photodynamic Therapy. *Biomaterials* **2019**, *218*, 119312.
(25) Simbula, G.; Columbano, A.; Ledda-Columbano, G.; Sanna, L.; Deidda, M.; Diana, A.; Pibiri, M. Increased ROS Generation and p53 Activation in α-Lipoic Acid-Induced Apoptosis of Hepatoma Cells. *Apoptosis* **2007**, *12*, 113−123.
(26) Ohashi, T.; Mizutani, A.; Murakami, A.; Kojo, S.; Ishii, T.; Taketani, S. Rapid Oxidation of Dichlorodihydrofluorescin with Heme and Hemoproteins: Formation of the Fluorescein is Independent of the Generation of Reactive Oxygen Species. *FEBS Lett.* **2002**, *511*, 21−27.
(27) Stennicke, H. R.; Renatus, M.; Meldal, M.; Salvesen, G. S. Internally Quenched Fluorescent Peptide Substrates Disclose the Subsite Preferences of Human Caspases 1, 3, 6, 7 and 8. *Biochem. J.* **2000**, *350*, 563−568.
(28) Lavrik, I. N.; Golks, A.; Krammer, P. H. Caspases: Pharmacological Manipulation of Cell Death. *J. Clin. Invest.* **2005**, *115*, 2665−2672.
(29) Porter, A. G.; Jänicke, R. U. Emerging Roles of Caspase-3 in Apoptosis. *Cell Death Differ.* **1999**, *6*, 99−104.
(30) Liu, Y.; Ma, K.; Jiao, T.; Xing, R.; Shen, G.; Yan, X. Water-Insoluble Photosensitizer Nanocolloids Stabilized by Supramolecular Interfacial Assembly Towards Photodynamic Therapy. *Sci. Rep.* **2017**, *7*, 42978−42985.
(31) Wang, Z.; Ma, G.; Zhang, J.; Yuan, Z.; Wang, L.; Bernards, M.; Chen, S. Surface Protonation/Deprotonation Controlled Instant Affinity Awitch of Nano Drug Vehicle (NDV) for pH Triggered Tumor Cell Targeting. *Biomaterials* **2015**, *62*, 116−127.
(32) Han, K.; Zhang, J.; Zhang, W.; Wang, S.; Xu, L.; Zhang, C.; Zhang, X.; Han, H. Tumor-Triggered Geometrical Shape Switch of Chimeric Peptide for Enhanced in Vivo Tumor Internalization and Photodynamic Therapy. *ACS Nano* **2017**, *11*, 3178−3188.
(33) Han, K.; Zhang, W. Y.; Zhang, J.; Lei, Q.; Wang, S. B.; Liu, J. W.; Zhang, X. Z.; Han, H. Y. Acidity-Triggered Tumor-Targeted Chimeric Peptide for Enhanced Intra-Nuclear Photodynamic Therapy. *Adv. Funct. Mater.* **2016**, *26*, 4351−4361.
(34) Lee, B. S.; Cho, Y. W.; Kim, G. C.; Lee, D. H.; Kim, C. J.; Kil, H. S.; Chi, D. Y.; Byun, Y.; Yuk, S. H.; Kim, K.; et al. Induced Phenotype Targeted Therapy: Radiation-Induced Apoptosis-Targeted Chemotherapy. *J. Natl. Cancer I.* **2015**, *107*, 1−9.

https://dx.doi.org/10.1021/acsabm.0c00122
ACS Appl. Bio Mater. XXXX, XXX, XXX−XXX